  Bull. Chem. Soc. Jpn., 65, 481—488 (1992)

Pressure-Dependent Intensity Anomalies in the $B^2\Sigma^+ \sim {}^4\Pi$ Perturbed Rotational Lines of the CN ($B^2\Sigma^+$-$X^2\Sigma^+$) 14-14 Band

Kazuhiro KANDA,† Haruhiko ITO,†† Kaoru SUZUKI,*,†††
Tamotsu KONDOW, and Kozo KUCHITSU*,††
Department of Chemistry, Faculty of Science, The University of Tokyo, Tokyo 113
†Department of Fundamental Science, College of Science and Engineering,
Iwaki Meisei University, Iwaki 970
††Department of Chemistry, Nagaoka University of Technology,
Nagaoka 940-21
†††Institute for Molecular Science, Myodaiji, Okazaki 444
(Received October 18, 1991)

The CN($B^2\Sigma^+$-$X^2\Sigma^+$) 14–14 emission band was observed in the reaction of Ar($^3P_{0,2}$) with BrCN by the use of the flowing afterglow method. The intensity anomalies in the rotational lines at $N'=7$ due to the $B^2\Sigma^+(v=14) \sim {}^4\Pi(v=7)$ perturbation were measured as a function of the pressure of Ar or He introduced as a collision partner in the reaction region, the ambient pressure being varied from 9 to 2000 mTorr (1 Torr=133.322 Pa). The intensities of the perturbed lines relative to that of the rotational band envelope increased with the ambient pressure in the low pressure region in the cases of both Ar and He. On the other hand, they decreased with pressure in the higher pressure region. The pressure dependence of the intensity anomaly for He followed that for Ar, although higher pressure of He was necessary to attain the same level of the intensity anomaly for Ar. These pressure dependences can be explained semiquantitatively by a model with collisional rotational relaxations in the quartet and doublet manifolds, the former being dominant at low ambient pressure and the latter at higher pressure.

A number of intensity anomalies have been observed in the CN($B^2\Sigma^+$-$X^2\Sigma^+$) emission in the reaction of cyanogen bromide with argon metastable atoms,[1-10]

$$Ar(^3P_{0,2}) + BrCN \longrightarrow CN(B^2\Sigma^+, {}^4\Pi, {}^4\Sigma^+, \text{etc.}) + Ar + Br. \quad (1)$$

These intensity anomalies are ascribed to the local perturbations between the $B^2\Sigma^+$ state and the $A^2\Pi_i$,[1,2,4,5,7,9] $^4\Sigma^+$,[3,6] and $^4\Pi$[6,8,9] states. Previous measurements on these intensity anomalies have shown that they are strongly pressure dependent,[1-4,8-10] indicating that rotational relaxation in the perturbing electronic states in collision with ambient argon atoms is prominent.

The pressure-dependent anomalies in the CN $B^2\Sigma^+ \sim A^2\Pi_i$ perturbed lines were first observed by Broida and co-workers[1,2] in the reactions of organic molecules with active nitrogen. A detailed analysis was made by Duewer et al.[3] on the pressure dependence of the rotational distribution of CN($B^2\Sigma^+$, $v=11$) with special attention to the anomalies due to the perturbation with $^4\Sigma^+$ in reaction (1) by the use of a steady-state kinetic model (see Appendix 2), by which the cross section for rotational relaxation in the $B^2\Sigma^+$ state by collision with Ar atoms was estimated to be 85±10 Å. However, they could not obtain direct evidence for collisional relaxation in the quartet manifold of the CN radical, mainly because their experiments had to be made at ambient pressures higher than 150 mTorr. Our recent study[10] has shown that these anomalies disappear at an ambient pressure below 9 mTorr and that the pressure dependence of the population enhancement of certain vibrational bands is attributable to collisional rotational relaxation with the ambient gas.

The purpose of the present study is to make more detailed measurements of the intensity anomalies in the rotational levels of the CN($B^2\Sigma^+$-$X^2\Sigma^+$) 14–14 band in argon and helium pressures ranging between 9 and 2000 mTorr and to analyze the pressure dependences to explain the origin of the observed anomalies. A two-state model is set up for this analysis by a modification of the steady-state kinetic model of Duewer et al.[3] to account for the rotational relaxations in the $B^2\Sigma^+$ and $^4\Pi$ states connected through strong perturbation.

Experimental

A flowing afterglow apparatus[10,11] was used. A flow tube was pumped by a mechanical booster pump (500 $dm^3 s^{-1}$). The flow velocity was measured to be ca. 300 $m s^{-1}$.[10] Argon metastable atoms were produced by microwave discharge (2.45 GHz, 100 W) in a Pyrex tube of 15 mm o.d. just before a stainless steal flow tube of 114 mm diameter. Charged species produced in the discharge were eliminated by applying an electric field between a pair of grids placed between the discharge region and the reaction zone. Cyanogen bromide was admixed to the flow ca. 15 cm downstream from the discharge region through a nozzle. Excited CN radicals were produced in reaction (1). The CN($B^2\Sigma^+$-$X^2\Sigma^+$) emission was observed perpendicularly to the direction of the gas flow through a quartz window and was focused on a Spex 1704 1-m monochromator with a slit of 10 μm×20 mm (spectral resolution: 0.1 Å FWHM). Dispersed emission was detected by a photomultiplier (Hamamatsu R585) and a photon-counting circuitry. The spectral response of the detection system was calibrated by the use of a standard halogen lamp (Ushio Electric Co.).

The lowest possible background pressure of Ar was 9 mTorr in the reaction zone to maintain a stable discharge in the Pyrex tube, whereas the pressure of the collision partner, Ar or He, which was introduced through an orifice on another flange, was varied from 0 to 2 Torr in the reaction zone. The pressure of rare gas was monitored by a Pirani gauge, which

was calibrated with a capacitance manometer (MKS Baratron).

The enhancement of the intensity anomalies in the 14–14 band increased as the distance between the sample nozzle and the observation point along the flow was increased. This is due to the collisional rotational relaxation that CN radicals suffer as they travel along the flow. In the present observation, the image of the entrance slit of the monochromator was set at a point only slightly downstream (less than 1 mm) from the sample injection nozzle by adjustment of a focusing lens so as to minimize the intensity anomaly and to eliminate the influence of collisional relaxation under these experimental conditions.

Results

Figure 1 shows the observed spectra of the perturbed rotational lines in the CN($B^2\Sigma^+$–$X^2\Sigma^+$) 14–14 band at different pressures of ambient argon. The rotational line at $N'=7$ splits into the extra and main lines due to the $B^2\Sigma^+\sim{}^4\Pi$ perturbation.[8,9,12] The wavefunctions of the perturbed levels are represented by[13]

$$\Psi_E=(1-\rho^2)^{1/2}\psi_\Pi-\rho^*\psi_\Sigma, \quad (2)$$

and

$$\Psi_M=\rho\psi_\Pi+(1-\rho^2)^{1/2}\psi_\Sigma, \quad (3)$$

where Ψ_E and Ψ_M represent the perturbed wavefunctions and ψ_Π and ψ_Σ are the unperturbed wavefunctions for the $^4\Pi$ and $B^2\Sigma^+$ states, respectively. The mixing parameter, ρ^2, that represents the character of the virtual $^4\Pi$ state in the perturbed states is reported to be 0.43.[8] The extra line corresponds to the transition from the perturbed rotational "E" level, which has more of the $^4\Pi$ state character. A schematic presentation of the perturbation between CN($B^2\Sigma^+$) and CN($^4\Pi$) is shown in Fig. 2.

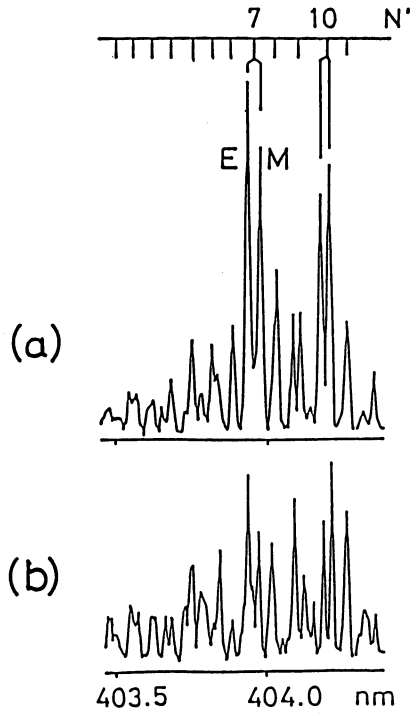

Fig. 1. Observed emission spectra of the 14–14 band of the CN($B^2\Sigma^+$) transition at Ar pressures of (a) 280 mTorr and (b) 9 mTorr.

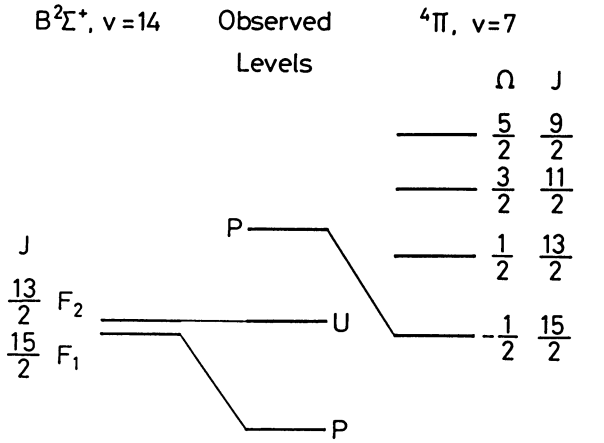

Fig. 2. Schematic representation of the perturbation between CN ($B^2\Sigma^+$) and CN ($^4\Pi$).

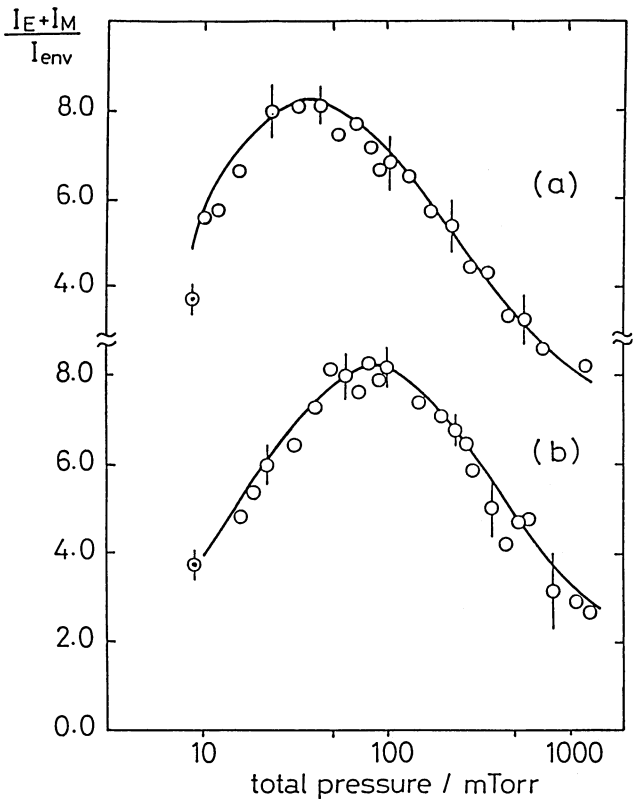

Fig. 3. Pressure dependence of the intensity ratio, $(I_E+I_M)/I_{env}$, in the $B^2\Sigma^+\sim{}^4\Pi$ perturbation with (a) Ar and (b) He as a collision partner. Open circles represent the observed values and the solid curve the best-fit simulation. Error bars represent one standard deviation. The value obtained with no additional collision partner through the second orifice is shown by a circle with a center dot (⊙).

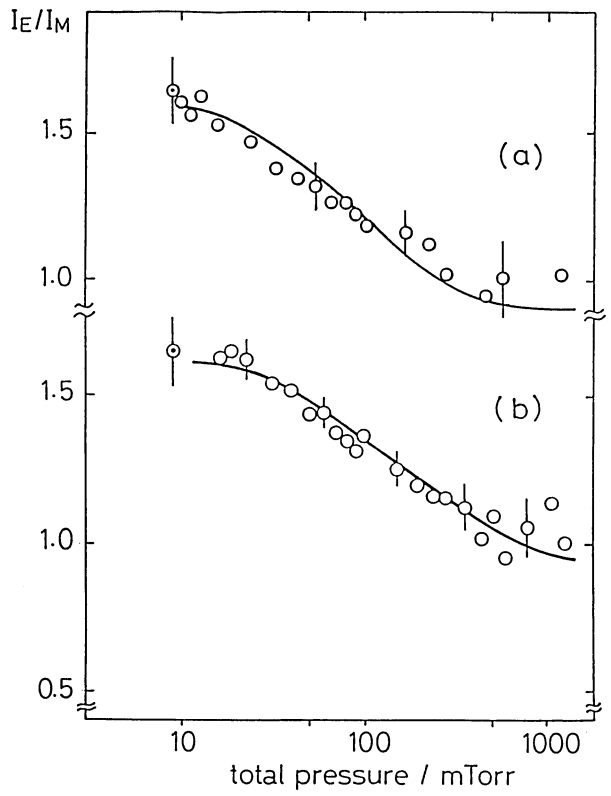

Fig. 4. Pressure dependence of the intensity ratio, I_E/I_M, in the $B^2\Sigma^+ \sim {}^4\Pi$ perturbation with (a) Ar and (b) He as a collision partner. See legend of Fig. 3.

Figure 3 shows the Ar and He pressure dependences of the observed intensity ratio, $(I_E+I_M)/I_{env}$, where I_M, I_E and I_{env} denote the intensities of the main, extra, and unperturbed rotational lines, respectively (see Fig. 1); I_{env} is estimated from the envelope of the vibrational band by interpolation. In Fig. 4 are shown the observed intensity ratios, I_E/I_M, for Ar and He as collision partners.

The pressure dependence shown in these Figures has the following features: (1) The intensities of the perturbed lines relative to that of the band envelope first increase and then decrease with the total pressure.[14] (2) The ratio of the intensity of the extra line to that of the main line decreases as the total pressure increases. (3) The observed intensity ratios, $(I_E+I_M)/I_{env}$ and I_E/I_M, in the case of He as a collision partner exhibit pressure dependences similar to those for Ar. (4) The maximum values of $(I_E+I_M)/I_{env}$ and I_E/I_M are the same for Ar and He; a higher pressure of He is required in order to achieve the same degree of rotational relaxation than that of Ar. As described in Discussion, the above observations can be reproduced by taking into account the rotational relaxation in the ${}^4\Pi$ and $B^2\Sigma^+$ states by collision with Ar and He atoms.

Discussion

Two-State Relaxation Model. In order to account for the observed characteristic pressure dependences, the following model of rotational relaxation is set up: The increase in the intensity anomalies observed in the low-pressure region with increasing ambient pressure is ascribed to the collisional rotational relaxation within the quartet manifold which populates the perturbed levels and the decrease in the anomalies in the high-pressure region to the increasing influence of the rotational relaxation in the B state.# A simulation based on this model is made by extension of the steady-state kinetic model of Duewer et al.[3] Intraelectronic pure rotational transitions and interelectronic transition only at the perturbed levels are included in the model, whereas collisional interelectronic transfer between the unperturbed rotational levels and a possible difference in the collision transfer rates for the spin-orbit states are ignored (See Appendix 1). As discussed in the following, this model reproduces the observed features by choice of a plausible set of adjustable parameters.

Formulation of Rotational Relaxation in Two Electronic States Connected through Perturbation. The collision-induced rotational relaxation within a single electronic state of the excited CN radical was analyzed by Duewer et al.[3] In their analysis the population Y is given by

$$Y=\sum_{m=0}^{\infty} A_m X_m, \tag{4}$$

where A_m is the probability that a radical experiences rotational-level-changing collisions m consecutive times and no further before its depletion by radiation or quenching from the system under consideration,

$$A_m=\left(\frac{\tau^{-1}+zQ}{\tau^{-1}+zQ+z}\right)\left(\frac{z}{\tau^{-1}+zQ+z}\right)^m, \tag{5}$$

and X_m is the population vector of the rotational levels after m rotational-level-changing collisions, with its component $X_m(N)$, where N is the rotational quantum number. The radiative lifetime is denoted as τ, and z is the collision frequency represented by

$$z=\sigma v_{rel} P_{tot}/kT, \tag{6}$$

where σ is the "total cross section" for collision-induced rotational relaxation, v_{rel} is the mean relative velocity between the CN radical and a collision partner, P_{tot} is the total pressure, and Q is the probability of the relaxation per collision to another vibrational or electronic state, relative to the rotational relaxation. This X_m is represented by the use of a collision matrix, P, as

The exact lifetime of the quartet state is not known, but it is expected to be orders of magnitude longer than that of the B state, considering a dark-state nature of the quartet state. This expectation is in accord with the features obtained by an ab initio calculation that the internuclear distance of the ${}^4\Pi$ state differs sigificantly from that of the ${}^4\Sigma^+$ state[15,16] and that the energy of the ${}^4\Pi$ state is close to that of the ${}^4\Sigma^+$ state.[15,16] Therefore, the effective number of collisions of the quartet state during its lifetime is larger than that of the B state during its lifetime of ca. 100 ns.

$$X_m = P^m X_0, \tag{7}$$

where P consists of the probability of relaxation per collision from N to N', $P_{NN'}$. From Eqs. 4—6, the cross section for rotational relaxation can be obtained from the measured population.

The applicability of the above treatment[3] is limited to a system that has a unique set of A_m, because without this constraint it is practically impossible to formulate A_m by taking into account all the rotational-level-changing collision paths. In the present analysis, however, A_m cannot be assumed to be unique, because two electronically excited states of CN are coupled through perturbation. In Ref. 2 the radiative lifetimes of the perturbed levels are derived by neglect of cross terms as

$$\tau_E^{-1} = (1-\rho^2)\tau_\Pi^{-1} + \rho^2\tau_\Sigma^{-1} \tag{8}$$

and

$$\tau_M^{-1} = \rho^2\tau_\Pi^{-1} + (1-\rho^2)\tau_\Sigma^{-1}. \tag{9}$$

The lifetime of a perturbed rotational level differs from those of unperturbed levels. Hence it is necessary to take into account the population transfer among the $B^2\Sigma^+$, $^4\Pi$, extra and main rotational levels, whose lifetimes are denoted as τ_Σ, τ_Π, τ_E, and τ_M respectively (see Eqs. 8 and 9). In addition, the cross sections for rotational relaxation for the $B^2\Sigma^+$ and $^4\Pi$ states are in general not identical. Therefore, the A_m's for the unperturbed levels of the doublet and quartet manifolds and the perturbed levels should be all different.

In order to deal with these circumstances, the following relaxation paths are taken into account by iteration: (1) emission from the unperturbed $B^2\Sigma^+$ levels, (2) collisional relaxations from the unperturbed $B^2\Sigma^+$ and $^4\Pi$ levels to the perturbed E and M levels, and (3) the repopulation of unperturbed levels by collisional transitions from the perturbed levels. The steady-state emission intensity is calculated by a summation of the emission intensities in repeated cycles of iteration. The detail of the calculation is described in Appendix 2 (see also Fig. A1).

Analysis of Pressure Dependence. The observed pressure dependence of the perturbed line was analyzed by the use of this model. The parameters α and β in the collisional relaxation probability (Eqs. A3 and A4) could not be determined simultaneously because of strong correlation between them. Therefore, the values reported in Ref. 3, $\alpha=0.2$ and $\beta=0.05$ were assumed. The observed ratios of $(I_E+I_M)/I_{env}$ and I_E/I_M were fitted to the calculated values. The fitting parameters were the lifetime of the state, the ratio of the formation rates to the $^4\Pi$ ($v=7$) and $B^2\Sigma^+$ ($v=14$) states, and the cross sections for rotational relaxation in the $^4\Pi$ ($v=7$) and $B^2\Sigma^+$ ($v=14$) levels. These cross sections are directly related to the effective collision frequency, which accounts for the rate of overall rotational relaxation (See Eq. 6 in conjunction with the rate equation Eq. A1 in Appendix 2). When the He atom is chosen as a collision partner, the collisional relaxation due to the Ar atoms which flow from the discharge region into the reaction zone must be taken into consideration in the low-pressure region. Accordingly, the collision frequency, z, in Eq. 6 is modified as

$$z = \sigma(\text{CN*–He})v_{rel}(\text{CN*–He})P_{He}/kT + \sigma(\text{CN*–Ar})v_{rel}(\text{CN*–Ar})P_{Ar}/kT, \tag{10}$$

where σ(CN*–He) and σ(CN*–Ar) represent the cross sections for rotational relaxation of the excited CN radical by collision with He and Ar, respectively, and v_{rel}(CN*–He) and v_{rel}(CN*–Ar) represent the mean relative velocities of the excited CN radical with respect to the He and Ar atoms, respectively. As shown in Figs. 3 and 4, the pressure dependences of the intensity anomalies obtained in the present experiment are reproduced reasonably well by the model described above by the use of the ratio of the formation rates, R_Π/R_Σ (See Eq. A9 in Appendix 2), of 2.4±0.8 and the rest of the parameters listed in Table 1.

Table 1. Parameters of Rotational Relaxation for CN by Collision with Argon and Helium Atoms[a]

	CN($^4\Pi$), $v=7$[b]	CN($B^2\Sigma^+$), $v=14$[b]
Cross section[c]		
with Ar	85(15) Å^2	95(15) Å^2
with He	24(5)	19(5)
Hard-sphere collision cross section[d]		
with Ar	44.7	45.6
with He	34.1	34.8
Lifetime	35(10) μs	[116 ns][e]

a) Numbers in parentheses represent one standard error to the last significant digit. b) The vibrational states are assigned in Ref. 12. c) From an analysis of the pressure dependence of the intensity anomalies by the two-state kinetic model. d) Estimated from a hard-sphere collision model. e) Ref. 33.

Since the lifetime of the $^4\Pi$ state is found to be two orders of magnitude longer than that of the $B^2\Sigma^+$ state, the rotational relaxation of the $^4\Pi$ state is dominant at low ambient pressure while that of the $B^2\Sigma^+$ state contributes at higher pressure. The observed increase in the $(I_E+I_M)/I_{env}$ at low ambient pressure is thus accounted for by the collisional rotational relaxation in the $^4\Pi$ state; the collisional relaxation to the perturbed level enhances the intensity anomaly. On the other hand, the decrease in the $(I_E+I_M)/I_{env}$ at higher pressure is due to the collisional rotational relaxation in the $B^2\Sigma^+$ state; in this case the enhanced population at the perturbed level is distributed among the rotational levels of the $B^2\Sigma^+$ state and, consequently, averaged out.

Collisional Rotational Relaxation by He and Ar. As shown in Figs. 3 and 4, the pressure dependence with He shifts from that with Ar to a higher pressure. This observation indicates that σ(CN*–He) is smaller than σ(CN*–Ar). An attempt is made to compare these "total cross sections" for rotational relaxation with the cross sections for hard-sphere collision estimated from

the van der Waals radii of the He and Ar atoms, 1.40 and 1.88 Å, respectively,[17] and the effective collision radii of CN($B^2\Sigma^+$) and CN($^4\Pi$), 1.89 and 1.93 Å, respectively. The effective radius of CN is estimated to be equal to the radius of a sphere whose volume is equal to that calculated from the van der Waals radii of C and N, 1.70 and 1.55 Å, respectively,[17] and the internuclear distances between the C and N atoms, 1.55 and 1.29 Å for $^4\Pi$ and $B^2\Sigma^+$ states, respectively, calculated from the rotational constants.[9] The estimates of these parameters seem reasonable because the cross sections thus derived, listed in Table 1, are similar to those for hard-sphere collision for Ar–N_2 and He–N_2, 37.8—38.5 and 30.5—31.4 Å^2 respectively, calculated by the use of the σ_{LJ} parameters of the Lennard-Jones (12, 6) potentials.[18–23]

The absolute values of the cross sections obtained in the present analysis depend on the choice of the collision matrix, P, and therefore on the assumed values of α and β in Eqs. A3 and A4. Nevertheless, it seems permissible to assume the same collision matrix for the collision of CN with Ar and He because rare gas atoms are isotropic. Therefore, the relative magnitude of the cross sections for Ar and He is taken for the following discussion. The ratio, $\sigma(CN^*\text{–Ar})/\sigma(CN^*\text{–He}) \approx 1.3$, derived from the above hard-sphere collision model is much smaller than that derived in the present study from the fitting of the observed pressure dependences, 3.5 for CN($^4\Pi$) and 5.0 for CN($B^2\Sigma^+$). The main origin of the discrepancy is thought to be the neglect of long-range interaction in the hard-sphere collision model. A simple calculation based on the electrostatic interaction between the permanent dipole moment of CN* and the induced dipole moment of Ar or He gives 6.0 for $\sigma(CN^*\text{–Ar})/\sigma(CN^*\text{–He})$. Thus long-range interaction seems to play a significant role in the collision-induced rotational relaxation.

This work was supported by the Joint Studies Program (1987—1988) of the Institute for Molecular Science. K. S. would like to thank the Itoh Science Foundation for partial financial support.

Appendix 1. Collision-Induced Transitions among Electronic and Spin-Orbit States.

Interelectronic Transitions. The collision-induced transitions between the unperturbed rotational levels of the $B^2\Sigma^+$ and $^4\Pi$ states are not included in the present simulation. Detailed state-to-state studies have been made by Dagdigian and co-workers[24–27] on a similar case of the CN $A^2\Pi_i$ and $X^2\Sigma^+$ states, where the rates of collisional interelectronic transitions are shown to be comparable or even faster than those of collisional intraelectronic pure rotational transitions. Hence, the "doorway" model that the interelectronic transitions through the perturbed levels are dominant is not operative in this particular molecular system. Unfortunately, the corresponding state-to-state transition rates are not available at present for the collisional rotational relaxation of the $^4\Pi$ state. It is highly unlikely, however, that the rates of collision-induced interelectronic transitions for the perturbed and unperturbed levels of the $^4\Pi$ state are similar to those for the levels of the $A^2\Pi_i$ state.[25] The pressure dependence of the intensity anomalies observed in the present study can hardly be expected if these rates are comparable. Moreover, the intensity anomalies cannot be reproduced in the simulation in our $B^2\Sigma^+$ and $^4\Pi$ system, even if a small contribution of the interelectronic collisional transition is taken into account. Therefore, the "doorway" model can be assumed in the present molecular system. This is attributable to a very short lifetime of the CN $B^2\Sigma^+$ state; once the CN $^4\Pi$ population is transferred in collisional interelectronic transition to the $B^2\Sigma^+$ state, hardly any back-transfer is possible from the $B^2\Sigma^+$ state to the $^4\Pi$ state and, hence, no contribution to the intensity anomalies of the perturbed levels is expected. A more quantitative treatment of the pressure dependence of the intensity anomalies must await the state-dependent cross sections of rotational transition provided by the state-to-state spectroscopic study of the $^4\Pi$ state.

Transitions between Spin-Orbit States. Collisional transitions between spin-orbit states have been extensively studied for a $^2\Pi$ state,[28–32] especially for collisions of NO,[28–30] CdH,[31] and CaF[32] with rare gas atoms. One of the major conclusions of these studies is that the cross sections for transitions between rotational levels belonging to different spin-orbit manifolds are smaller than those for transitions within a given spin-orbit manifold. A consensus seems to have been reached that the former is roughly an order of magnitude smaller than the latter,[29–32] although an earlier paper[28] reports that it holds only for the NO–He case. Unfortunately, a similar study for a $^4\Pi$ state has not yet been made. It seems to be a reasonable assumption, however, that a similar "propensity" rule holds for a $^4\Pi$ state. Thus, only the transitions within a given spin-orbit manifold are included in the present simulation analysis.

Appendix 2. Procedure of Iteration.

Relaxation in a Single Electronic State. Prior to the discussion on the two-state problem, the case of a single state[3] is summarized. The rate equation for the population of the N-th rotational level, $X(N)$, is written as

$$dX(N)/dt = F(N) - X(N)/\tau + z\sum_{N'}[P_{N'N}X(N') - P_{NN'}X(N)] - zQX(N). \quad (A1)$$

Here $F(N)$ is the formation rate of the N-th rotational level of a given vibrational state. The definitions of τ, z, and Q are given in Discussion. The normalized initial population of the N-th rotational level, $X_0(N)$, is given by

$$X_0(N) = F(N)/\sum_N F(N), \quad (A2)$$

where the subscript zero indicates that no collisional relaxation has taken place. Duewer et al.[3] tested three models for $P_{NN'}$ and concluded that their experimental data were best reproduced by the following exponential-gap model

$$P_{NN'} = c(\alpha^{|N-N'|} + \beta)[(2N'+1)/(2N+1)], \quad (N>N') \quad (A3)$$

$$P_{NN'} = c'(\alpha^{|N-N'|} + \beta)[(2N'+1)/(2N+1)] \exp(-\Delta E_{NN'}/kT), \quad (N<N') \quad (A4)$$

and

$$P_{NN}=0. \tag{A5}$$

In Eq. A4, $\Delta E_{NN'}$ denotes the difference in the rotational energies between the N-th and N'-th levels, α and β are adjustable parameters, and c and c' are normalization constants so that

$$\sum_{N'} P_{NN'}=1. \tag{A6}$$

Initial Populations. The relative rates of formation of the unperturbed levels in the $^4\Pi$ or $B^2\Sigma^+$ state can be represented as

$$F_\Lambda(N)=(2S_\Lambda+1)f_\Lambda(N), \tag{A7}$$

wheres S_Λ is the total spin of the respective electronic state ($\Lambda=\Sigma$ for the $B^2\Sigma^+$ state and $\Lambda=\Pi$ for the $^4\Pi$ state) and N is the rotational quantum number. The rates of formation of the unperturbed rotational levels of the spin-sublevels of the $^4\Pi$ and $B^2\Sigma^+$ states, $f_\Lambda(N)$, are assumed to follow the Boltzmann function,

$$f_\Lambda(N)=r_\Lambda(2N+1)\exp(-E_\Lambda(N)/kT_{rot})/\sum_N(2N+1)\exp(-E_\Lambda(N)/kT_{rot}). \tag{A8}$$

Here, r_Λ is the rate of formation of the spin-sublevel; the rate of formation of the vibronic state in question, R_Λ, is represented as

$$R_\Lambda=(2S_\Lambda+1)r_\Lambda. \tag{A9}$$

The rotational energy of the level specified by N in the $^4\Pi$ or $B^2\Sigma^+$ state is denoted by $E_\Lambda(N)$. The effective rotational temperature of $B^2\Sigma^+$, T_{rot}, is set to 2100 K, the higher effective rotational temperature of the double Boltzmann distribution observed in the CN($B^2\Sigma^+$-$X^2\Sigma^+$) 14-14 band,[10] because the fractional population for the lower rotational temperature is small. The effective rotational temperature of the $^4\Pi$ state is not available at present; hence it is tentatively assumed to be equal to that of $B^2\Sigma^+(v=14)$. It is further assumed that all the spin-orbit states are produced in equal probability. The initial population of the rotational level N, populated at a unit time interval, Δt, is set equal to its formation rate:

$$U_\Sigma^{0,0}(N)=f_\Sigma(N)\Delta t. \tag{A10}$$

As to the notation of $U_\Lambda^{i,j}(N)$, superscript i represents the number of collisional transitions between the unperturbed and perturbed levels, and j represents the number of collisions causing rotational relaxation among the unperturbed levels in a single vibronic state. The relative rates of formation of the perturbed levels, which correspond to their initial populations, can be written as

$$f_E=(1-\rho^2)f_{\Pi P}+\rho^2 f_{\Sigma P}, \tag{A11}$$

and

$$f_M=\rho^2 f_{\Pi P}+(1-\rho^2)f_{\Sigma P}, \tag{A12}$$

where

$$f_{\Lambda P}=f_\Lambda(N_P). \tag{A13}$$

Relaxation and Radiative Decay in the $B^2\Sigma^+$ State. The population of the CN radicals in the $B^2\Sigma^+$ state which decay by radiation before relaxation to a perturbed level is calculated. The relaxation processes under consideration are illustrated in Fig. A1(a). The partial population of the CN radicals after

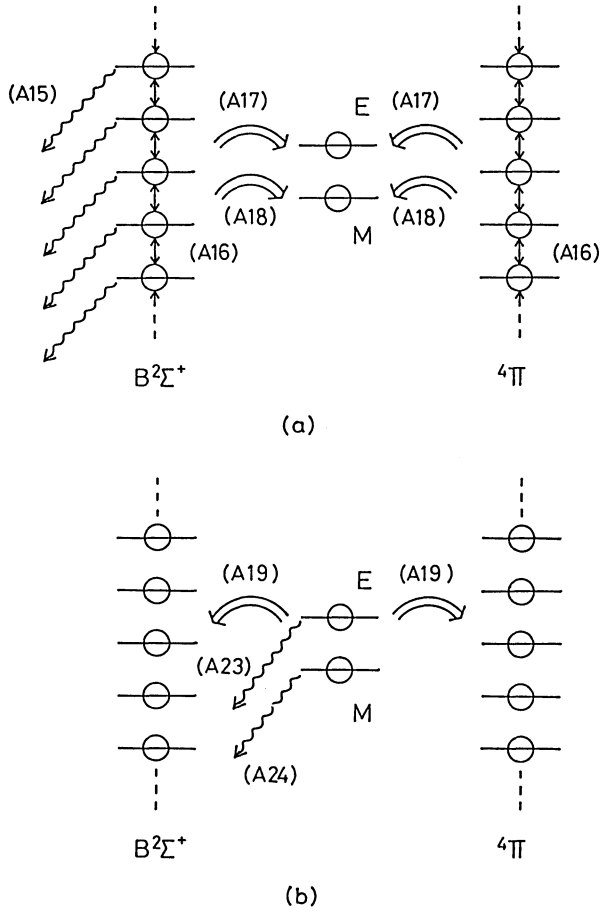

Fig. A1. Schematic presentation of the relaxation paths: (a) relaxation and radiative decay in the $B^2\Sigma^+$ and $^4\Pi$ states, (b) relaxation and radiative decay relevant to the perturbed levels. Iteration was made for (a) and (b). The numbers in parentheses in the figure represent the corresponding numbers in the equations displayed in Appendix 2.

the j-th collision and before the $(j+1)$-th collision is given by

$$V_\Sigma^{0,j}=\frac{\tau^{-1}}{\tau^{-1}+zQ+z}U_\Sigma^{0,j}(N). \tag{A14}$$

The subscript and superscripts in $V_\Lambda^{i,j}(N)$ are defined equally to those in $U_\Lambda^{i,j}(N)$. The population after the $(j+1)$-th collision, $U_\Sigma^{0,j+1}(N)$, is determined from $U_\Sigma^{0,j}(N)$ as follows: 1) The product of $U_\Sigma^{0,j}(N)$ and the probability matrix, whose components are given in Eqs. A3—A5, is calculated. 2) A "propensity" rule is assumed to apply for the collisional transitions between the spin sublevels that the transitions are restricted in the same spin-orbit manifold, e.g. $\Delta\Omega=0$ for a case (a) molecule as in the CN $^4\Pi$ state in the present analysis. It is then shown that

$$U_\Sigma^{0,j+1}=\frac{z}{\tau^{-1}+zQ+z}PU_\Sigma^{0,j}. \tag{A15}$$

The calculation is terminated when the number of consecutive collisions j is so large that the population of the excited CN radicals that survive after more than j collisions, $U_\Sigma^{0,j}(N)$, is negligible and that no further change is observed in the computed pressure dependence.

The population which is transferred by collision from other unperturbed rotational levels in the $B^2\Sigma^+$ state to the virtual level which participates in perturbation is calculated as

$$T_{\Sigma P}{}^0 = \sum_j \frac{z}{\tau^{-1}+zQ+z} \sum_N P_{N,N_p} U_\Sigma{}^{0,j}. \quad \text{(A16)}$$

The same treatment for the population is made for the $^4\Pi$ state, and the population $T_{\Pi P}{}^0$, which is formed by relaxation from the rotational levels in the $^4\Pi$ state to the perturbed level, is calculated.

Populations for Perturbed Levels. The population of the CN radical which emits radiation from the perturbed levels is calculated. The processes under consideration is illustrated in Fig. A1(b). The nascent populations of the perturbed levels, populated at a unit time interval, Δt, that correspond to the extra and main lines, $U_E^{0,0}$ and $U_M^{0,0}$, are given by

$$U_E^{0,0} = (1-\rho^2) T_{\Pi P}{}^0 + \rho^2 T_{\Sigma P}{}^0 + f_E \Delta t \quad \text{(A17)}$$

and

$$U_M^{0,0} = \rho^2 T_{\Pi P}{}^0 + (1-\rho^2) T_{\Sigma P}{}^0 + f_M \Delta t \quad \text{(A18)}$$

where the third terms are omitted in further iterations. The procedure for calculating $U_E^{0,0}$ and $U_M^{0,0}$ is similar to that described above for $U_\Sigma{}^{0,0}(N)$. As a result, a part of the CN radicals emit radiation from the perturbed levels, and the rest of them are relaxed to unperturbed levels in the $^4\Pi$ and $B^2\Sigma^+$ states. These populations, $T_{P\Sigma}{}^0$ and $T_{P\Pi}{}^0$, which are formed by relaxation to the $B^2\Sigma^+$ and $^4\Pi$ states, respectively, before radiation from the perturbed levels are substituted for $U_\Sigma{}^{1,0}(N)$ and $U_\Pi{}^{1,0}(N)$ for a subsequent cycle of iteration as

$$U_\Lambda{}^{1,0} = P T_{P\Lambda}, \quad \text{(A19)}$$

where

$$T_{P\Lambda}(N) = 0 \quad \text{for } N \neq N_p \quad \text{(A20)}$$

and

$$T_{P\Lambda}(N) = T_{P\Lambda} \quad \text{for } N = N_p. \quad \text{(A21)}$$

Calculation of the Emission Intensities. A further calculation is made on the populations of the unperturbed levels in the $B^2\Sigma^+$ state, $\sum_j U_\Sigma{}^{1,j}(N)$ and the $^4\Pi$ state, $\sum_j V_\Pi{}^{1,j}(N)$, and those lost by relaxation to the perturbed levels, $U_{\Sigma P}{}^1$ and $U_{\Pi P}{}^1$. The above procedure is repeated until the population U becomes negligible. The overall populations, V_E, V_M, and V_{env} are calculated, by summation over all the possible collisional relaxation routes, to be

$$V_E = \sum_i \sum_j V_E{}^{i,j}, \quad \text{(A22)}$$

$$V_M = \sum_i \sum_j V_M{}^{i,j}, \quad \text{(A23)}$$

and

$$V_{env} = [\sum_i \sum_j V_\Sigma{}^{i,j}(N_p-1) + \sum_i \sum_j V_\Sigma{}^{i,j}(N_p+1)]/2, \quad \text{(A24)}$$

where, $V_E{}^{i,j}$ and $V_M{}^{i,j}$ are calculated in a similar manner as in Eq. A14.

It is to be noted that in our experimental setup the CN(B) radicals produced upstream from the observation point may contribute to the observed emission. Therefore, Eqs. A22—A24 weighted with a temporal profile should be integrated along the line of flow down to the observation point. The corrected population is represented by

$$X \propto V\tau[1-\exp(-d/v\tau)], \quad \text{(A25)}$$

where v is the flow velocity and d is the distance along the flow. The right-hand side of Eq. A25 being expanded, the population is expressed as

$$X \propto Vd/v, \quad \text{(A26)}$$

by neglecting higher-order terms, since $d/v\tau \ll 1$ because d is small under the present experimental conditions. Finally, the overall emission intensities are calculated by

$$I_E \propto V_E/\tau_E, \quad \text{(A27)}$$

$$I_M \propto V_M/\tau_M, \quad \text{(A28)}$$

and

$$I_{env} \propto V_{env}/\tau_\Sigma. \quad \text{(A29)}$$

References

1) H. P. Broida and S. Golden, *Can. J. Chem.*, **38**, 1666 (1960).
2) H. E. Radford and H. P. Broida, *J. Chem. Phys.*, **38**, 644 (1963).
3) W. H. Duewer, J. A. Coxon, and D. W. Setser, *J. Chem. Phys.*, **56**, 4355 (1972).
4) J. A. Coxon, D. W. Setser, and W. H. Duewer, *J. Chem. Phys.*, **58**, 2244 (1973).
5) J. A. Coxon, D. A. Ramsay, and D. W. Setser, *Can. J. Phys.*, **53**, 145 (1975).
6) A. J. Yencha, Y. Ozaki, T. Kondow, and K. Kuchitsu, *Chem. Phys.*, **51**, 343 (1980).
7) Y. Ozaki, T. Nagata, K. Suzuki, T. Kondow, and K. Kuchitsu, *Chem. Phys.*, **80**, 73 (1983).
8) Y. Ozaki, H. Ito, K. Suzuki, T. Kondow, and K. Kuchitsu, *Chem. Phys.*, **80**, 85 (1983).
9) H. Ito, Y. Ozaki, T. Nagata, T. Kondow, and K. Kuchitsu, *Can. J. Phys.*, **62**, 1586 (1984).
10) K. Kanda, H. Ito, K. Someda, K. Suzuki, T. Kondow, and K. Kuchitsu, *J. Phys. Chem.*, **93**, 6020 (1989).
11) I. Nishiyama, Y. Ozaki, K. Suzuki, and K. Kuchitsu, *Chem. Phys. Lett.*, **67**, 258 (1979).
12) H. Ito, Y. Ozaki, K. Suzuki, T. Kondow, and K. Kuchitsu, *Chem. Phys. Lett.*, **139**, 581 (1987).
13) A. T. Wager, *Phys. Rev.*, **64**, 18 (1943).
14) K. Kanda, H. Ito, K. Suzuki, T. Kondow, and K. Kuchitsu, unpublished results. A similar pressure dependence as in Fig. 4 was observed in the intensity anomalies in the CN $A^2\Pi_i(v=10) \sim B^2\Sigma^+(v=0)$ and $^4\Sigma^+ \sim B^2\Sigma^+(v=11)$ perturbations when Ar was used as a collision partner.
15) H. Ito, Y. Ozaki, T. Nagata, T. Kondow, K. Kuchitsu, K. Takatsuka, H. Nakamura, and Y. Osamura, *Chem. Phys.*, **98**, 81 (1985).
16) P. J. Bruna, H. Dohmann, and S. D. Peyerimhoff, *Can. J. Phys.*, **62**, 1508 (1984).
17) A. Bondi, *J. Phys. Chem.*, **68**, 441 (1964).
18) M. D. Pattengill, R. A. La Budde, R. B. Bernstein, and C. F. Curtiss, *J. Chem. Phys.*, **55**, 5517 (1971).
19) F. P. Tully and Y. T. Lee, *J. Chem. Phys.*, **57**, 866 (1972).
20) M. H. Alexander, *J. Chem. Phys.*, **67**, 2703 (1977).
21) S.-I. Chu and A. Dalgarno, *J. Chem. Phys.*, **63**, 2115 (1975).
22) W. Erlewein, M. von Seggern, and J. P. Toennies, *Z.*

Phys., **211**, 35 (1968).
23) H. P. Butz, R. Feltgen, H. Pauly, and H. Vehmeyer, *Z. Phys.*, **247**, 70 (1971).
24) N. Furio, A. Ali, and P. J. Dagdigian, *Chem. Phys. Lett.*, **125**, 561 (1986).
25) A. Ali, J. Guo, and P. J. Dagdigian, *Chem. Phys. Lett.*, **131**, 331 (1986).
26) N. Furio, A. Ali, and P. J. Dagdigian, *J. Chem. Phys.*, **85**, 3860 (1986).
27) G. Jihua, A. Ali, and P. J. Dagdigian, *J. Chem. Phys.*, **85**, 7098 (1986).
28) A. S. Sudbo and M. M. T. Loy, *J. Chem. Phys.*, **76**, 3646 (1982).
29) T. Orlikowski and M. H. Alexander, *J. Chem. Phys.*, **79**, 6006 (1983).
30) H. Joswig, P. Andresen, and R. Schinke, *J. Chem. Phys.*, **85**, 1904 (1986).
31) J. Defayard and O. Nedelec, *Chem. Phys.*, **71**, 279 (1982).
32) C. Dufour, B. Pinchemel, M. Douay, J. Schamps, and M. H. Alexander, *Chem. Phys.*, **98**, 315 (1985).
33) D. C. Cartwright and P. J. Hay, *Astrophys. J.*, **257**, 383 (1982).